On electric field measurements based on intensity ratio of 1 − and 2 + systems of nitrogen in discharges with high specific deposited energy

N D Lepikhin, N A Popov, S M Starikovskaia

On electric field measurements based on intensity ratio of 1^- and 2^+ systems of nitrogen in discharges with high specific deposited energy.

N. D. Lepikhin[1,2], N. A. Popov[3], S. M. Starikovskaia[1]

[1] Laboratory of Plasma Physics (CNRS, Ecole Polytechnique, Univ. Paris-Sud, Observatoire de Paris, Sorbonne Université, l'Institut Polytechnique de Paris), Ecole Polytechnique, route de Saclay, 91128 Palaiseau, France

[2] Institute for Plasma and Atomic Physics, Ruhr University Bochum, 44780 Bochum, Germany

[3] Skobeltsyn Institute of Nuclear Physics, Moscow State University, Moscow, 119991, Leninsky gory, Russia

E-mail: nikita.lepikhin@rub.de, svetlana.starikovskaia@lpp.polytechnique.fr

Abstract. Analysis of optical emission spectroscopy (OES) in application to the measurements of the electric field has been performed for the nanosecond capillary discharge in molecular nitrogen at moderate gas pressure at high specific energy deposition. Significant discrepancy between results of electric field measurements by OES technique and capacitive probe measurements is demonstrated. Decay rates of excited species as well as rotation structure of corresponding optical transitions are used to identify possible population/depopulation channels of $N_2^+(B^2\Sigma_u^+, v')$ and $N_2(C^3\Pi_u, v')$ states. Kinetic calculations taking into account additional quenching of $N_2^+(B^2\Sigma_u^+, v')$ and $N_2(C^3\Pi_u)$ states by electrons, additional population $N_2^+(B^2\Sigma_u^+)$ by electron impact from the ground state of the molecular ion and by a reaction of excited $N_2(A^3\Sigma_u^+)$ with the ground state of N_2^+ describes adequately behavior of experimentally measured emission of both considered systems.

Keywords: electric field, emission spectroscopy, kinetics, capillary nanosecond discharge in nitrogen

1. Introduction

Measurement of the electric field by optical emission spectroscopy (OES) has been discussed over the last five decades [1–3]. The core idea of the technique is to measure the ratio of intensities of two optical transitions with different thresholds/cross-sections and to relate this ratio, knowing the dependence of rates of excitation by electron impact, radiative lifetime and the quenching rates, with the field value. For air or nitrogen, these transitions are $0-0$ or $2-5$ vibrational transitions of the second positive system (SPS) $N_2(C^3\Pi_u, v') \rightarrow N_2(B^3\Pi_g, v'')$, and $0-0$ transition of the first negative system (FNS) $N_2^+(B^2\Sigma_u^+, v') \rightarrow N_2^+(X^2\Sigma_g^+, v'')$. In [4], a wider set of $(0-2)$, $(1-4)$, $(2-5)$ SPS transitions was considered for more accurate electric field determination. The time-dependent equation relating reduced electric field value with evolution of the measured FNS and SPS emission intensities, I_B and I_C, is the following (see [5] for details):

$$\frac{k_B(E/N)\cdot A_B}{k_C(E/N)\cdot A_C} = \frac{\frac{dI_B}{dt} + \frac{I_B}{\tau_B}}{\frac{dI_C}{dt} + \frac{I_C}{\tau_C}}. \tag{1}$$

Here τ_B and τ_C are the effective life times (due to radiative decay and collisional quenching) of the levels $N_2^+(B^2\Sigma_u^+, v')$ and $N_2(C^3\Pi_u, v')$ respectively, A_B and A_C are the Einstein coefficients for corresponding vibrational-vibrational transitions and $k_B(E/N)$ and $k_C(E/N)$ are the rate constants of excitation by direct electron impact from the ground state of nitrogen, $N_2(X^1\Sigma_g^+)$. The left hand side of the equation (1) is a function of the reduced electric field, while the right hand side is a experimentally measured value.

In nitrogen and air (i) when the field is uniform in space or when the emission of both selected states comes from the same discharge region; (ii) for a quasi-stationary problem or when the temporal behavior of derivatives of emission intensity over time is taken into account; (iii) at the conditions of excitation from the ground state of molecular nitrogen by direct electron impact (in absence of any stepwise excitation); (iv) when the decay of the emitting states can be described only by natural radiative decay and collisional quenching by N_2 and O_2 molecules, the technique of the electric field measurements based on the ratio of emission of selected molecular bands is validated both experimentally and theoretically.

Nanosecond discharges at moderate pressures, below 30 Torr and low specific deposited energy, 0.01 eV/molecule or lower, developing in the form of the fast ionization waves (FIWs) represent a classical example of discharges with high amplitude fast-changing electric fields [5, 6] where the conditions (i)-(iv) are valid in the region after the FIW front where the non-local effects are not important. Electric field in the FIWs has been measured by different techniques; results for the E-field obtained by OES are in reasonable agreement with the data obtained by capacitive probes [5, 6] and recently developed [7] electric field induced second harmonic generation of a short pulsed laser radiation (E-FISH).

There are various discharges, where the conditions (i)-(iv) are not fulfilled. High

pressure discharges often represent a system of thin plasma channels having the regions with high spatial gradients of the electric field. The scale of the spatial non-uniformity at atmospheric pressure is 5-50 μm, as for the plasma in the vicinity of the dielectric in surface dielectric barrier discharges (DBDs) [8] or in the head of the volumetric streamer [9,10]. The authors of [10] have shown numerically that the peak of the electric field in the streamer head is not located at the same position as the maximum of the excitation rates for the SPS and FNS emissions, and that the use of quasi-steady-state and local in space OES technique results in overestimate of the E-field in the head of the streamer by a factor of two. Different delays of excitation of SPS and FNS were studied experimentally and numerically in [11] as well.

If the OES technique is applied to the fast changing in time electric field, the time derivative of the emission should be taken into account [5,6,12], but it is important that the changes of the field are slow enough so that the EEDF follows the field. This is a necessary and sufficient condition to use the theoretical approach.

If the empirical formulae of the ratio of emission of the SPS (0-0 transition at $\lambda = 337$ nm and 2-5 transition at $\lambda = 394.3$ nm) and the emission the FNS (0-0 transition at $\lambda = 391.4$ nm) as a function of E/N suggested on the basis of experiments in a Townsend DC discharge [13] are used, the condition transforms to a more strict demand of a quasi-stationarity of the problem in the sense that the time derivatives of the intensity of emission should be small comparing to radiative decay and quenching (that is $dI/dt \ll I/\tau$ in the equation (1)). Comparison of different approaches of taking or not into account the derivative is analyzed in [14] for nanosecond discharge at very high overvoltage in atmospheric pressure air. It should be noted the results of the E-field measurements based on (1) and the empirical formula suggested in [13] are extremely sensitive [15–17] to the quenching rate constants of the emitting states. The best agreement between these two approaches was obtained [15] using the quenching rates [18, 19] measured in the afterglow of nanosecond pulsed discharge. Analysis of available in the literature data on emission cross sections for the electron-impact excitation, radiative lifetimes, and quenching rate constants for $N_2(C^3\Pi_u, v' = 0)$ and $N_2^+(B^2\Sigma_u^+, v' = 0)$ states can be found in [20, 21].

If not only the direct electron impact but some other processes are responsible for excitation of the molecular bands of interest, an additional kinetic analysis of validity of the OES technique is required. Such analysis was done in the near afterglow of short pulsed discharges, where the additional population of $N_2(C^3\Pi_u)$ comes from lower triplet states of nitrogen [22], in moderate pressure AC discharges where the additional population of $N_2^+(B^2\Sigma_u^+)$ is due to excitation from He* metastables in He:N_2 mixture [23], or in atmospheric pressure gliding arc in nitrogen, where the additional population of $N_2^+(B^2\Sigma_u^+)$ is explained by electron impact excitation of the ground state of molecular ion [24]. Vibrational exchange within $N_2(C^3\Pi_u, v' = 0-4)$ manifold and the confidence interval for the cross-sections of excitation of these levels by direct electron impact are analyzed in [4].

Additional population of $N_2^+(B^2\Sigma_u^+)$ results in abnormally high intensities of the

FNS comparing to the intensity of the SPS. This effect is often observed in discharges at high specific deposited energies [24,25]. Extremely high ratio of FNS and SPS was also observed ahead of the front of ionization wave and near the HV electrode in atmospheric pressure nanosecond discharge in air with a very high overvoltage, $U = 85$ kV [14]. Similar discrepancy between the OES electric field measurements and data derived from electrical measurements was observed in [26] at much smaller voltage amplitudes for pin-to-pin nanosecond discharge in air: in the vicinity of the cathode, the OES-measured E-field significantly, by a factor of 3-4, exceeded the E-field derived from the voltage measurements.

Additional depopulation processes, similarly to additional population channels mentioned above, strongly affect the results of the OES electric field measurements. The assumption about the quenching of excited levels of interest by the main neutral components of the mixture is wrong if additional species with high rate constants of collisions with $N_2(C^3\Pi_u)$ and $N_2^+(B^2\Sigma_u^+)$ are efficiently produced in a plasma. Abnormally fast decay of $N_2(C^3\Pi_u)$ due to quenching by electrons was observed in the nanosecond capillary discharge with high reduced electric fields and high specific deposited energies at moderate pressure [27]. This discharge was the subject of the previous studies [27–30]. A good agreement between the electrical fields obtained by 2D numerical modeling [28] and experimentally measured by capacitive probe [27, 28] provides a solid prove for the measured electric field waveform. Detailed 1D numerical modeling reproducing the experimentally measured electric field, plasma decay, decay of nitrogen excited species, gas temperature dynamics and nitrogen atom density evolution [27, 29, 30] shows a good understanding of the discharge kinetics. Thus, nanosecond capillary discharge is chosen in the present work to demonstrate the peculiarities of electric field measurements based on FNS and SPS ratio at conditions of high deposited energy.

2. Experimental setup

The discharge was initiated in a quartz capillary tube with the internal diameter of 1.7 mm and the external one of 3.0 mm, inter-electrode distance was 75 mm, see figure 1 (a).

High voltage(HV) pulse of positive polarity 18.6 kV in amplitude on the electrode, 30 ns FWHM and 4 ns rise time applied to the high-voltage electrode of the discharge cell via 25-m long coaxial cable at repetition rate of 10 Hz.

The waveforms of the high voltage pulse and the deposited energy were measured using custom made calibrated back current shunts (BCS). The waveforms of the high voltage pulse coming from the generator, U_{inc}, and of the high voltage pulse reflected from plasma, U_{refl}, were measured by BCS1; the waveform of the high voltage transmitted through the plasma, U_{trans}, was recorded by BCS2. The attenuation of the signal propagating in the high voltage cable was taken into account. The waveform of the voltage applied to the HV electrode calculated as $(U_{inc} + U_{refl})$ is shown in figure 1 c

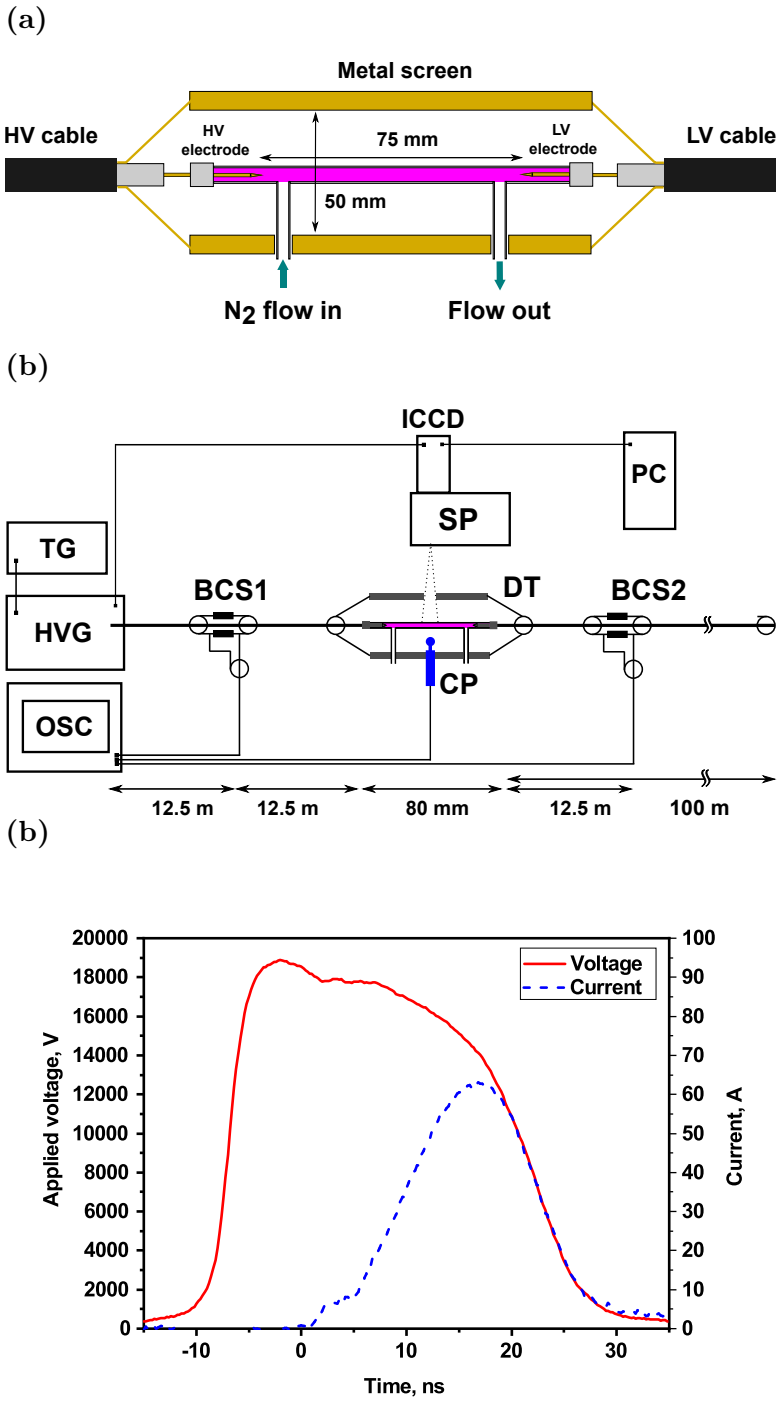

Figure 1. (a) Schematic view of the discharge cell used in the experiments; (b) The general scheme of the experimental setup with the main experimental equipment. TG is triggering generator, HVG is a high voltage generator, OSC is oscilloscope, BCS is back current shunt, CP is capacitive probe, DT is discharge tube, PMT is photomultiplier tube, ICCD is intensified charge–coupled device (camera), SP is spectrometer, PC is personal computer; (c) The voltage applied to the HV electrode together with the current transmitted through the discharge.

together with the current transmitted through the discharge.

The longitudinal electric field was measured by two methods: by a custom-made calibrated capacitive probe (CP) [6, 28, 31–35] and by the back current shunts. The capacitive probe is a detector of electric potential. The potential in plasma as a function of the distance x from the high voltage electrode was measured at different x moving the probe in the slit of the metal screen along the discharge tube. The data were taken each 1 mm, and the map of electric potential was constructed for any time instant. The electric field was calculated as a gradient of the measured electric potential. Back current shunts provide absolute value of the electric field after closing the discharge gap in assumption that the distribution of potential is uniform along the discharge gap [28].

The optical emission from the discharge was collected by the UV Fused Silica lens to the 100 μm entrance slit of the spectrograph with 500 mm focal length (Acton SP-2500i, Princeton Instruments, 1200 l/mm grating). The light was detected by the ICCD camera (PI-MAX 4 1024i, Princeton Instruments). The spectra were corrected according to the spectral sensitivity of the system. A long-pass colored glass filter FGL400 (Thorlabs) was used to avoid the second order of diffraction in the measurements at the wavelengths higher than 400 nm. The matching of the sensitivity levels of two parts of the spectrum taken with/without the filter was controlled by superimposition of the spectra overlapping at the region 400-420 nm.

The pure nitrogen from Air Liquid with admixtures < 5.5 ppm was used for the experiments. The gas bottle was connected to the discharge tube through a flow controller (Brooks Instrument 5850TR). The flow rate was equal to 50 sccm to assure the gas renewal between the discharge pulses. Gas pressure in the middle of the capillary was measured as a mean value of reading of two capacitive-type pressure gauges (CMR 362, Pfeiffer Vacuum) installed upstream and downstream of the tube, and was equal to 27 mbar. For more detailed description of the experimental setup and the discharge please refer to [27–30, 36].

3. Spectroscopic measurements: intensities of 1^- and 2^+ systems of nitrogen

A typical optical emission spectrum of the nanosecond capillary discharge in pure nitrogen at $P = 27$ mbar is presented in figure 2. The signal is collected during the entire discharge pulse, the camera gate is equal to 60 ns. The transitions corresponding to the first negative system (FNS) of molecular nitrogen $N_2^+(B^2\Sigma_u^+, v') \rightarrow N_2^+(X^2\Sigma_g^+, v'')$ are denoted as $N_2^+(v'-v'')$. The transitions corresponding to the second positive system (SPS) of nitrogen $N_2(C^3\Pi_u, v') \rightarrow N_2(B^3\Pi_g, v'')$ are denoted as $(v'-v'')$. The transitions corresponding to the first positive system (FPS) of molecular nitrogen $N_2(B^3\Pi_g, v')$ $\rightarrow N_2(A^3\Sigma_u^+, v'')$ are highlighted by a blue frame in figure 2(d). The emission of the second positive system dominates in the spectrum. The highest amplitude of the signal corresponding to the SPS(0-0) transition is about 1080 a.u., while the highest amplitude corresponding to the FNS(0-0) transition is about 34 a.u.

The ratio of intensities of the first negative and the second positive systems is

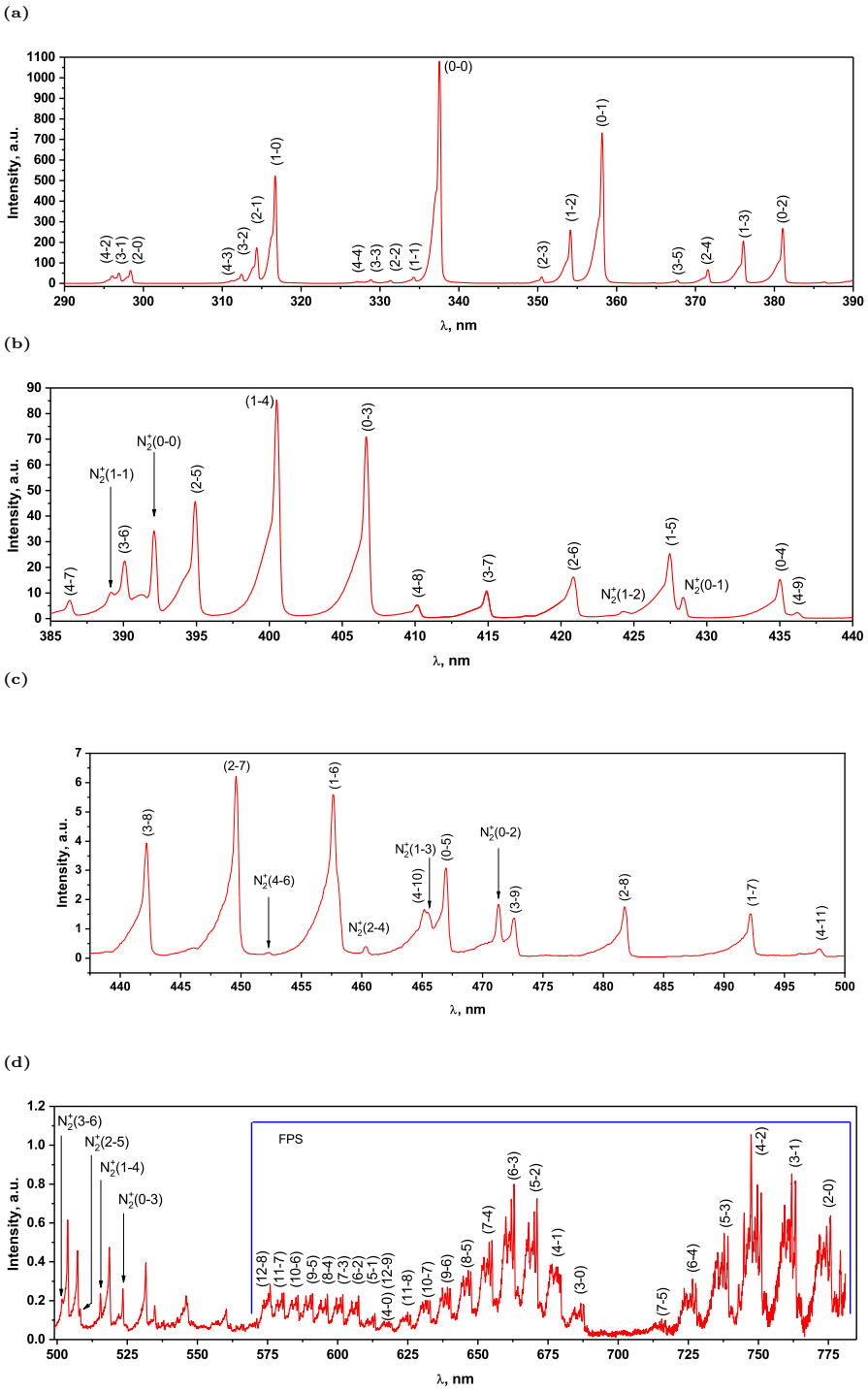

Figure 2. Typical spectrum of the nanosecond capillary discharge in wavelength range (a) 290-390 nm, (b) 385-440 nm, (c) 440-500 nm, (d) 500-780 nm. For notations see text. The signal is collected during the whole pulse. Entrance slit of 100 μm, 600 l/mm grating, averaging of 100 accumulations. Pure nitrogen, 27 mbar.

different for the time-resolved measurements. Time-resolved spectra of the SPS(2-5), FNS(0-0) and SPS(0-0) emission are compared in figures 3 and 4, presenting spectra taken during a few first nanoseconds of the discharge with a camera gate of 1 ns. The

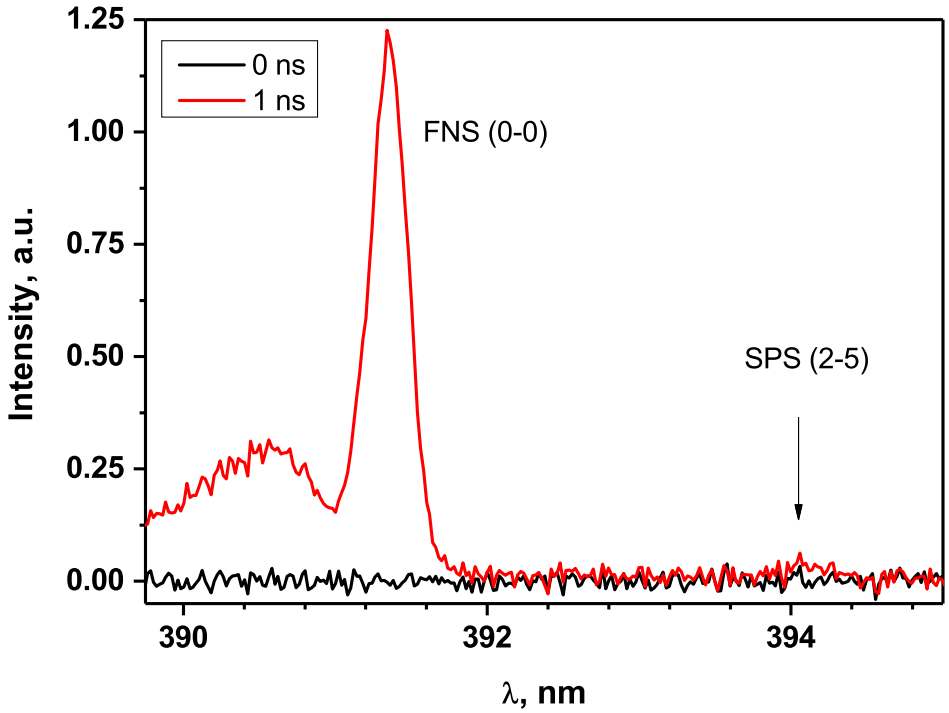

Figure 3. SPS(2-5) and FNS(0-0) transitions during the first nanosecond of the discharge (red curve). The signal corresponding to the one nanosecond before the discharge (noise) is given for comparison (black curve). Pure nitrogen, 27 mbar. Entrance slit of 100 μm, 1200 l/mm grating, averaging of 200 accumulations.

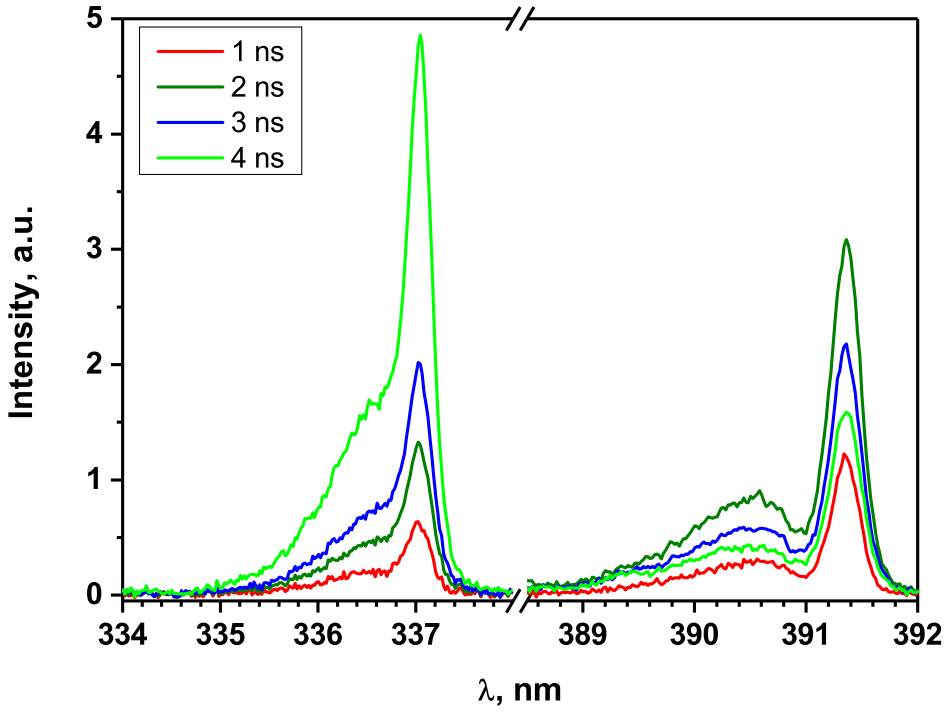

Figure 4. SPS(0-0) and FNS(0-0) transitions during first four nanoseconds of the discharge. Pure nitrogen, 27 mbar. Entrance slit of 100 μm, 1200 l/mm grating, averaging of 200 accumulations.

spectra of the FNS(0-0) and SPS(2-5) bands at the time interval $1-30$ and $31-55$ ns can be found in the Appendix A. During the first nanosecond of the discharge, the amplitude of the FNS(0-0) transition is more than 20 times higher than the amplitude of the SPS(2-5) transition (figure 3) and approximately two times higher than the intensity of the SPS(0-0) transition (figure 4). First nanoseconds of the emission correspond to the ionization wave front. If it is assumed that both $N_2(C^3\Pi_u)$ state (electronic energy is 11.05 eV [37]) and $N_2^+(B^2\Sigma_u^+)$ state (electronic energy is 18.74 eV [37]) are populated by direct electron impact from the ground state of molecular nitrogen, the high ratios $R_{391/394}$ and $R_{391/337}$ indicate that E/N should be rather high. The amplitudes of the FNS(0-0) and SPS(0-0) transitions become comparable after 3 ns. After 4 ns the amplitude of the SPS(0-0) transition is much higher than one of the FNS(0-0) transition.

To get the emission intensity as a function of time, overlapped spectra of the FNS(0-0) and SPS transitions were separated. Corresponding bands were fitted by SpecAir software [38] and individually integrated over the wavelength.

Dependence of the emission intensity as a function of time is presented in figure 5. It is clearly seen that the maximum intensity of the SPS(0-0) transition is 20 times higher than the maximum intensity of the FNS(0-0) transition (see the time interval $10-25$ ns). The intensity of the FNS(0-0) transition dominates in the beginning of the discharge, corresponding to the front of the fast ionization wave.

In order to obtain reduced electric field value from the measurement results shown in figure 5 the corresponding terms $Y = dI/dt + I/\tau$ from the right hand side of equation (1) should be calculated first. The results of this calculation are presented in figure 6.

Negative values of $Y_{SPS(0-0)}$, $Y_{SPS(2-5)}$ and $Y_{FNS(0-0)}$ are clearly seen in figure 6. The negative values indicate that there are additional depopulation mechanisms of the considered excited levels, which are not taken into account by "classical" plasma kinetics, when the effective life time τ is calculated as a result of radiative decay and collisional quenching by background gas only. Even positive values of Y can be underestimated leading to incorrect results. To illustrate this, the electric field was calculated by (1) using the ratio $Y_{SPS(0-0)}$ and $Y_{FNS(0-0)}$ shown in figure 6 (the cross-sections from [39] are used to calculate $k_B(E/N)$ and $k_C(E/N)$). The results are presented in figure 7 together with electric field measured by capacitive probe [27], E/N is calculated taking into account the initial gas temperature of 380 K, see figure 11 a. Please note, that the OES results are shown *only to demonstrate* significance of *a possible error* of this approach at conditions of high specific energy deposition. It also should be noted that at a few first nanoseconds (0-3 ns) the value of the E-field obtained by OES exceeds E-field measured by capacitive probe by a factor of 5. A possible explanation is high radial electric fields [28, 40] in the front of FIW, while a capacitive probe provides the longitudinal component of the electric field. Also, finite spatial resolution of the capacitive probe, in combination with a finite velocity of the discharge front, about 1.5 cm s^{-1} [28], limits precision of the measurements during such transient event as fast ionization wave propagation. Therefore, the front of the discharge is out of the subject of discussion of the present work and the electric fields obtained by different techniques are

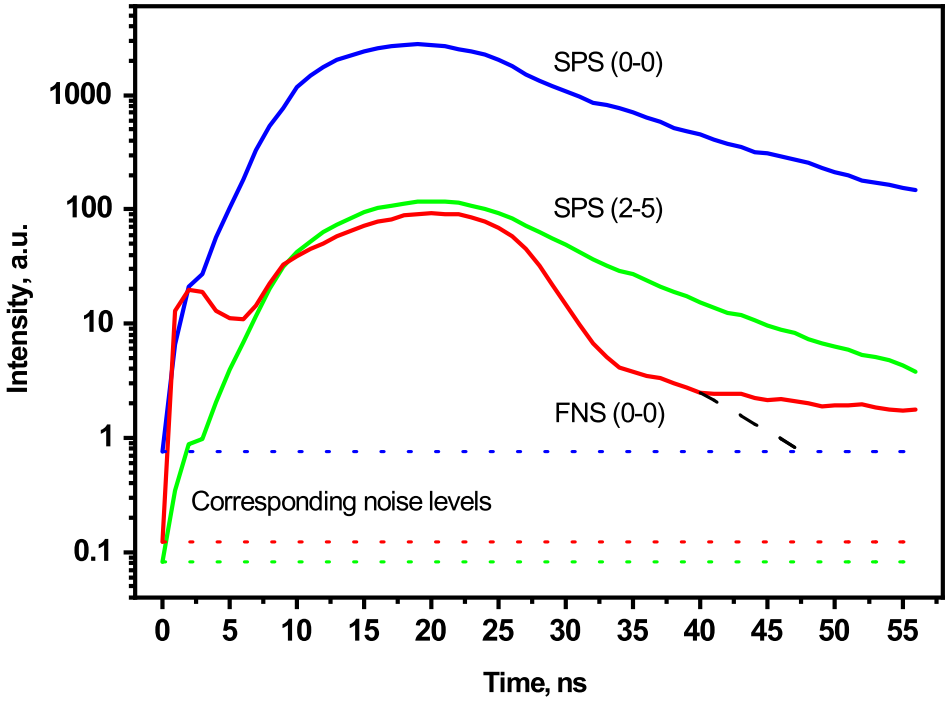

Figure 5. The intensities of the SPS(0-0), SPS(2-5) and FNS(0-0) transitions during time instants 1-55 ns. The horizontal dot lines indicate the corresponding noise levels defined as the signal intensity at 0 ns. The dash line corresponds to the decay of the $N_2^+(B^2\Sigma_u^+, v' = 0)$ state calculated based on the quenching rate constants measured in [18]. The difference between the FNS (0-0) dynamics and the calculated decay is attributed to an additional population of the $N_2^+(B^2\Sigma_u^+, v' = 0)$ state, see Discussion. Pure nitrogen, 27 mbar.

compared only after the breakdown. It is clearly seen in figure 7 that E/N obtained by OES based technique is initially underestimated and then is significantly overestimated and has even an opposite trend after 10 ns if it is compared with capacitive probe results. The reason is an abnormally fast decay of excited species due to quenching by electrons observed in the same discharge [27]. Once the electron density is high enough [27], the role of this additional decay process becomes significant and affects the population of excited states, which is not taken into account in calculations of $Y_{FNS(0-0)}$, $Y_{SPS(0-0)}$ and $Y_{SPS(2-5)}$, see Section 5. It should be emphasized that when both $Y_{FNS(0-0)}$ and $Y_{SPS(0-0)}$ (or $Y_{SPS(2-5)}$) are negative, their ratio is positive and mechanical use of formula (1) (by data treatment script, for example) will still provide some field value, although it would be completely wrong, see figure 7, where electric field values are returned by (1) at 25-35 ns, while both $Y_{SPS(0-0)}$ and $Y_{FNS(0-0)}$ are nonphysically negative.

The experimental data shown in figure 5 also shows that the decay of the intensity of the FNS(0-0) transition, and so the decay of the density of $N_2^+(B^2\Sigma_u^+, v' = 0)$ state, slows

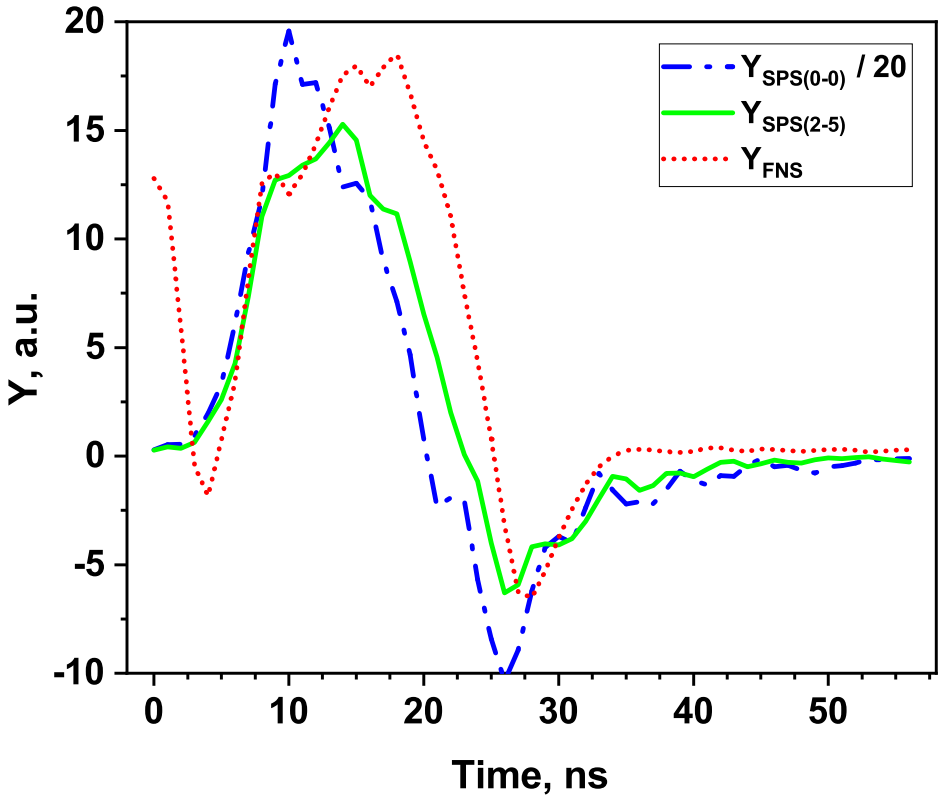

Figure 6. Terms $Y = dI/dt + I/\tau$ calculated for SPS(0-0) (dash-dot), SPS(2-5) (solid) and FNS(0-0) (dot-dot) transitions, where I is corresponding emission intensity from figure 5. The effective life times, τ, are calculated based on the quenching rate constants measured in [18]. Pure nitrogen, 27 mbar.

down in the late afterglow significantly and becomes even slower (the observed life time is about 28 ns) than the decay predicted theoretically according to the quenching rate constants measured in [18] (the effective life time is 6.4 ns at 27 mbar). This indicates that besides the additional quenching channel there is an additional population process of the $N_2^+(B^2\Sigma_u^+, v' = 0)$ state, which also can affect the results of OES measurements of the electric field.

Such additional kinetic processes are consequence of high excitation degree in the discharge with high energy deposition at high reduced electric fields. Thus, it is recommended to analyze the waveforms of the emission intensity separately for the given conditions. A special attention should be paid to the decay rates: if they do not correspond to the decay related to the radiative lifetime and quenching by the main components of the gas mixture, this should be analyzed and taken into account. Such analysis for the present conditions is performed it the following sections.

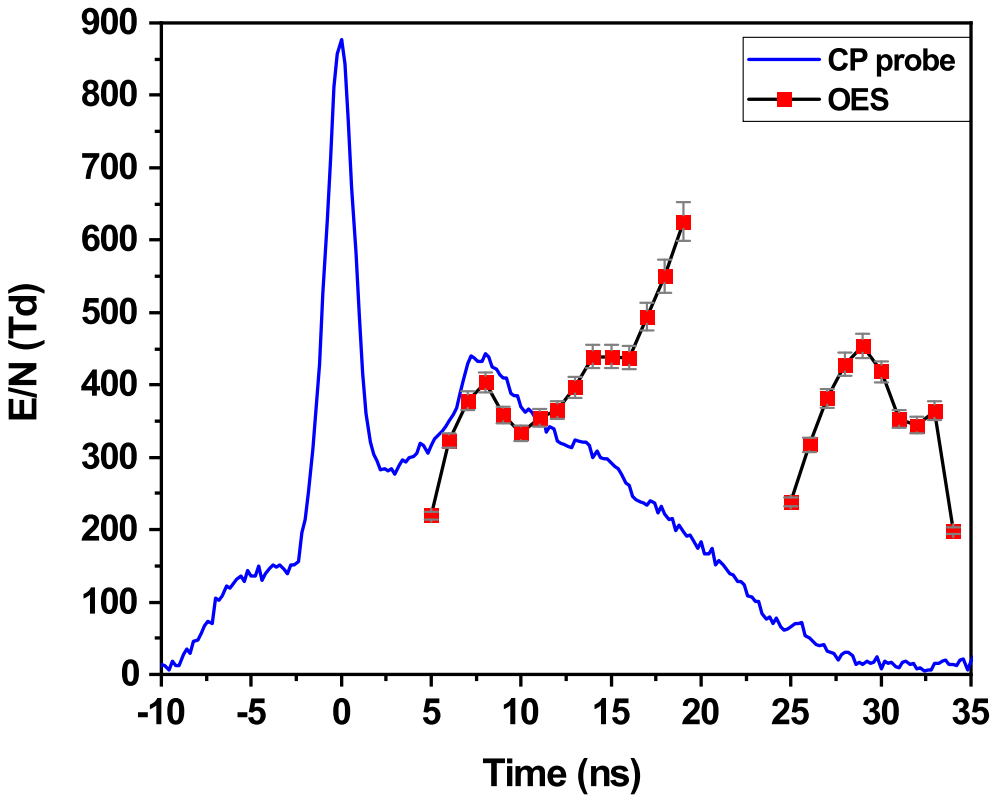

Figure 7. Electric field measured by capacitive probe together with the results of OES technique. Please note, that the OES results are shown only to demonstrate significance of possible error of this approach at conditions of high specific energy deposition. The error bars correspond to a stochastic error caused by noise in the experimental data.

4. Numerical kinetics modeling

To study the processes influencing the measurements of reduced electric field based on ratio of intensities of 1^- and 2^+ systems of nitrogen in discharges with a high excitation degree, the experimental results were compared with the results of numerical calculations. The kinetics calculations were performed for the region of measurements situated in the middle of the discharge tube, 37 mm apart from the high voltage electrode. Taking into account the axial symmetry of the problem, the calculations were made in 1D approximation. Initial electron density distribution, $N_e(r)$, obtained on the basis of experimentally measured emission distribution for the same conditions [29], was taken as input data for the code together with the measured waveform of the transmitted current, $I_{trans}(t)$.

The following main neutral species were included in the model: $N_2(X^1\Sigma_g^+)$, $N_2(A^3\Sigma_u^+)$, $N_2(B^3\Pi_g)$, $N_2(W^3\Delta_u)$, $N_2(B'^3\Sigma_u^-)$, $N_2(C^3\Pi_u)$, $N_2(a'^1\Sigma_u^-)$, $N_2(a^1\Pi_g)$, $N(^4S)$,

$N(^2D)$, $N(^2P)$. Three levels, $N_2(B^3\Pi_g)$, $N_2(W^3\Delta_u)$ and $N_2(B'^3\Sigma_u^-)$, were considered and designated as a single effective $N_2(B)$ level.

Ionization and excitation rates were calculated for each time instant as a function of the reduced electric field on the basis of solution of the Boltzmann equation in a two–term approximation using BOLSIG+ code [41] with the cross–sections taken from [42]. It should be noted that behind the front of the discharge, in the region of the main energy input, typical reduced electric field does not exceed a few hundreds of Td and so the two–term approximation is valid [42–44].

The $e-e$ processes were taken into account in the calculations, since at the end of the pulse, at relatively high electron densities $n_e \sim 10^{15}$ cm^{-3} [27] and low electric fields, $E/N < 100$ Td, the electron–electron collisions become important for EEDF formation, electron drift velocity and rates of excitation for considered electronically excited states.

The basis of the kinetic model is the reactions described in detail and analyzed in [45, 46]. Results of the verifications related to the role of the associative ionization in nitrogen plasma are presented in [45, 47], reactions of nitrogen dissociation by electron impact at conditions of high and low degree of vibrational excitation of N_2 molecules were analyzed in [46] and [48], respectively. The role of the reactions of step-wise dissociation of electronically excited states $N_2(A^3\Sigma_u^+, B^3\Pi_g, C^3\Pi_u)$ in discharges with high ionization degree was considered in [30]. In [29] the processes of fast gas heating in nitrogen plasma at high ionization degree and high specific energy deposition was presented. Obtained results were used for fine tuning of the kinetic model of a gas-discharge nitrogen plasma, which is particularly important for the present conditions.

The model was validated by comparison of the calculated and measured waveforms of the reduced electric field. The experimental value was obtained with the help of calibrated capacitive probe. A good agreement between numerical modeling and experiment has been achieved [27].

Densities of the key species shown in figure 8 and in figure 10 (see the next section) demonstrate high excitation degree caused by high specific deposited energy at high reduced electric fields. This leads to more complex plasma kinetics, which can be important for applications. For example, mentioned above step-wise dissociation of excited nitrogen states $N_2(A^3\Sigma_u^+, B^3\Pi_g, C^3\Pi_u)$ by electron impact allows to achieve high dissociation degree of molecular nitrogen, see figure 8, which agrees well with the experimentally measured value [30].

5. Discussion

In this section the key processes influencing application of OES for $E-$field measurements at high deposited energy are discussed. To analyze the emission curves presented in figure 5, the densities of the upper electronic states of the SPS(0-0), $[N_2(C^3\Pi_u, v' = 0)]$, and of the FNS(0-0), $[N_2^+(B^2\Sigma_u^+, v' = 0)]$, were calculated numerically as a function of time.

During the discharge excitation of the SPS of molecular nitrogen takes place by

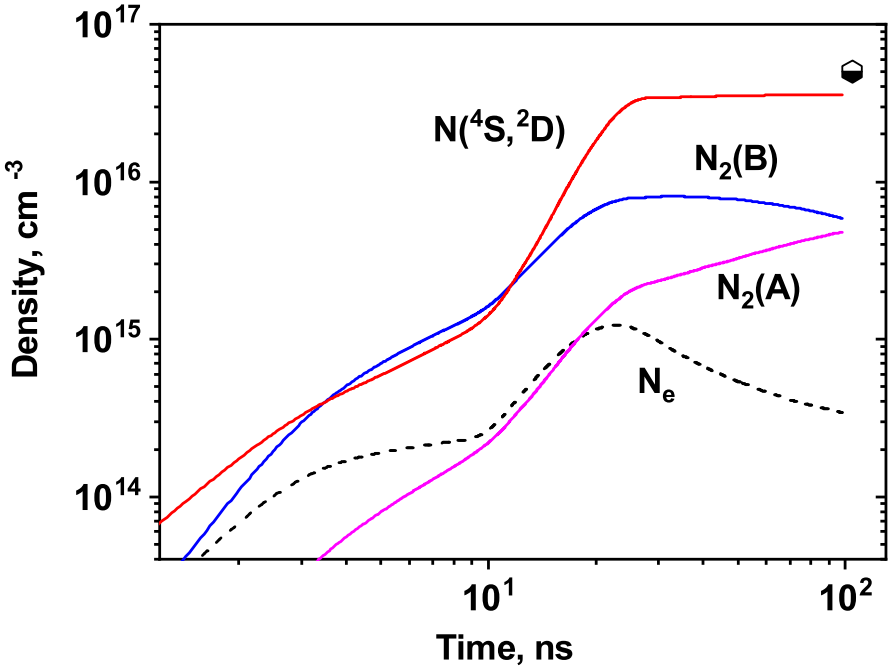

Figure 8. Temporal evolution of electron density and density of electronically-excited particles averaged over the discharge cross-section (curves). Symbol corresponds to the experimental data [30]. Pure nitrogen, 27 mbar.

direct electron impact from the ground state of molecular nitrogen:

$$\mathrm{N_2(X^1\Sigma_g^+)} + e \rightarrow \mathrm{N_2(C^3\Pi_u)} + e, \tag{2}$$

since the discharge time scale is too short to consider any other population channels of $\mathrm{N_2(C^3\Pi_u)}$. For example, additional population by vibrational relaxation of $\mathrm{N_2(C^3\Pi_u}, v'' > 0)$ states recently suggested by [4] is not relevant at the conditions of present work: the time of vibrational relaxation of $\mathrm{N_2(C^3\Pi_u}, v = 1, 2)$ is about 110-120 ns. It should also be noted that the main population of $\mathrm{N_2(C^3\Pi_u)}$ in the discharge afterglow occurs in the self-quenching reaction of $\mathrm{N_2(A^3\Sigma_u^+)}$ molecules and during the electron-ion recombination $\mathrm{N_4^+} + e \rightarrow \mathrm{N_2(C^3\Pi_u)} + \mathrm{N_2}$ [49].

The decay of a given electronic state, in case of *low* specific deposited energy discharges at moderate pressure, is determined by the radiative decay and by the quenching by background gas only. As it was mentioned above, in the nanosecond capillary discharge at *high* specific deposited energy, the additional quenching by electrons should be taken into account [27]:

$$\mathrm{N_2(C^3\Pi_u)} + e \rightarrow \mathrm{N_2(X^1\Sigma_g^+, A^3\Sigma_u^+, B^3\Pi_g)} + e, \tag{3}$$

$$\mathrm{N_2(C^3\Pi_u)} + e \rightarrow \mathrm{N(^2D)} + \mathrm{N(^4S)} + e. \tag{4}$$

At $E/N = 150 - 250$ Td (figure 7), the rate constant of the quenching by electrons to lower electronic states N_2 is high as $1.5 \cdot 10^{-7}$ cm^{3}s^{-1}, see figure 9, where de-excitation rates are shown as function of reduced electric field. The corresponding cross-sections are calculated based on detailed-balance principle as reverse processes to excitation by direct electron impact from lower electronic states with corresponding cross-sections taken from [50] and EEDFs calculated by BOLSIG+ software [41]. The rate constant of $N_2(C^3\Pi_u)$ dissociation is also high, about $1.0 \cdot 10^{-7}$ cm^{3}s^{-1} [30]. At $N_e > 2 \cdot 10^{14}$ cm^{-3} the quenching by electrons becomes the dominant channel of $N_2(C^3\Pi_u)$ deactivation. Neglecting this process, in particular, explains non-physical behavior of calculated values of $Y_{SPS(0-0)}$ and $Y_{SPS(2-5)}$ shown in figure 6.

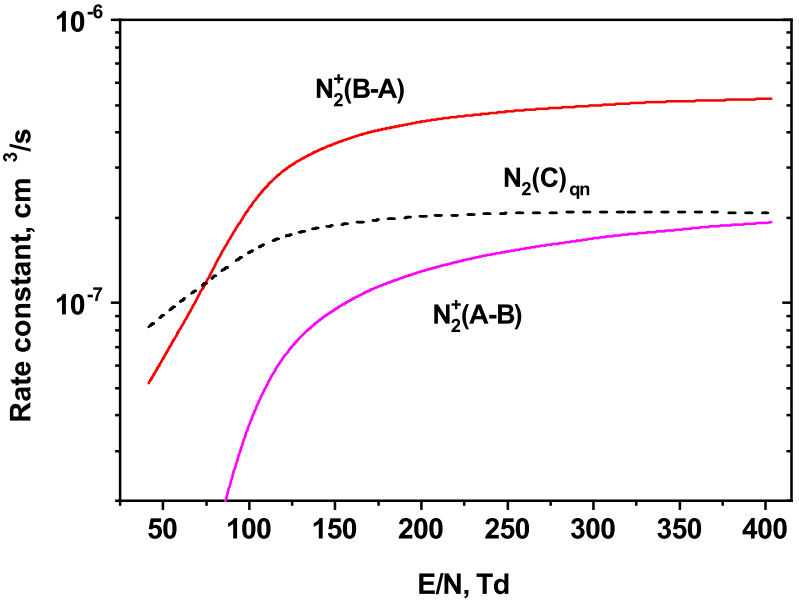

Figure 9. Rate constants of the quenching of the $N_2(C^3\Pi_u)$ and the $N_2^+(B^2\Sigma_u^+)$ states by electrons and rate constant of the excitation of the $N_2^+(B^2\Sigma_u^+)$ state from the $N_2^+(A^2\Pi_u)$ state as functions of reduced electric field in pure nitrogen. The corresponding cross-sections are calculated based on detailed-balance principle as reverse processes to excitation by direct electron impact from lower electronic states with corresponding cross-sections taken from [50] and EEDFs calculated by BOLSIG+ software [41].

Taking into account the reactions (3) and (4) together with the reactions of population by direct electron impact (2), radiative decay and quenching by N_2 molecules provides an excellent agreement between measured and calculated behavior of the SPS, see figure 10.

As it was mentioned above, while the rate constants of the quenching of the $N_2(C^3\Pi_u)$ state obtained in different works are in good agreement between each other, the rate constants of the quenching of the $N_2^+(B^2\Sigma_u^+)$ state, k_q^B, differ significantly [16]. In the present work the best agreement with the experimentally measured dynamics of

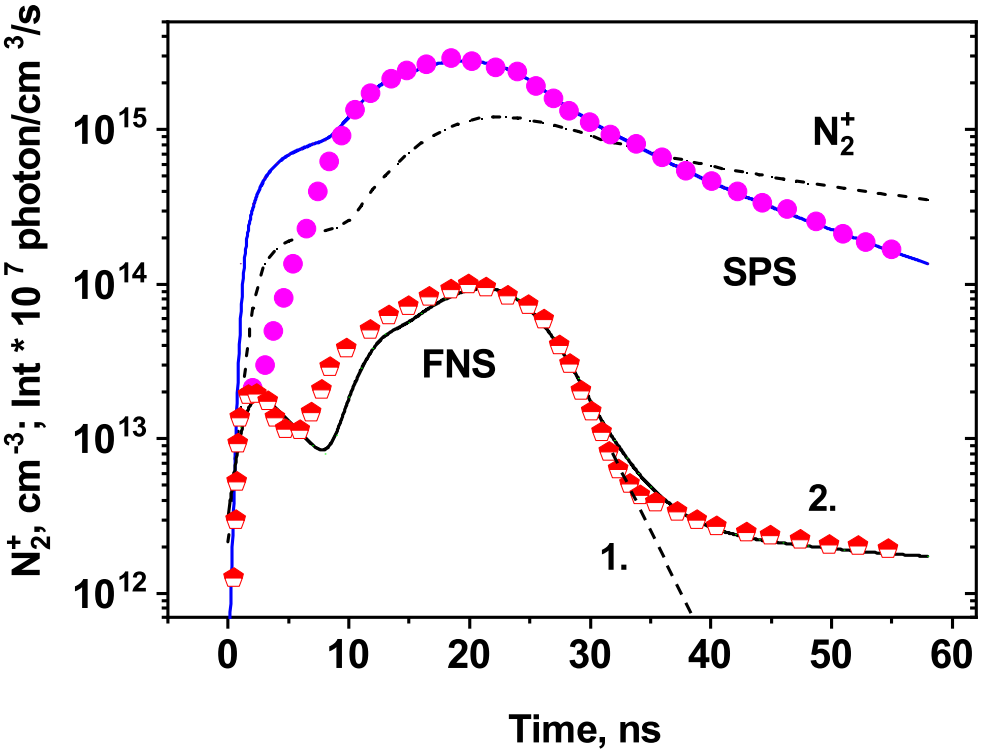

Figure 10. Dynamics of N_2^+ density averaged over tube cross-section and emission intensity of FNS and SPS of molecular nitrogen calculated numerically (lines): without (1) and with (2) process (12) included, see text. Experimental data from figure 5 in arbitrary units are given for comparison (symbols). Pure nitrogen, 27 mbar.

the FNS(0-0) emission at $t = 25 - 35$ ns is achieved at collisional quenching frequency corresponding to $k_q^B = 7 \cdot 10^{-10}\text{cm}^3\text{s}^{-1}$. The results are shown in figure 10. It should be noted that this value of k_q^B exceeds the value of the rate constant of the quenching of the $N_2^+(B^2\Sigma_u^+)$ state by nitrogen obtained in [18], which provides the best agreement with the measurements results of [13] (see the calculations performed with the collisional-radiative model used in the present work in Appendix B). A probable reason of such discrepancy is the quenching of $N_2^+(B^2\Sigma_u^+)$ state by electrons, which can be rather intensive, see figure 9, due to high ionization degree. It should be noted that at $E/N \geq 150$ Td reaction rates of $N_2^+(B^2\Sigma_u^+)$ quenching to $N_2^+(A^2\Pi_u)$ and the reversed excitation process are very high, so an equilibrium of populations of these states is achieved rather quickly. However, at decreasing reduced electric fields the excitation $N_2^+(A^2\Pi_u) \rightarrow N_2^+(B^2\Sigma_u^+)$ decreases significantly, so the depopulation dominates, see figure 9.

Population of $N_2^+(B^2\Sigma_u^+)$ state *additional* to the excitation of $N_2^+(B^2\Sigma_u^+)$ by direct electron impact in collisions with the background N_2 molecules:

$$N_2(X^1\Sigma_g^+, v' = 0) + e \rightarrow N_2^+(B^2\Sigma_u^+, v'' = 0) + e + e, \qquad (5)$$

can increase ratio of FNS and SPS intensities as well.

The presence of the additional $N_2^+(B^2\Sigma_u^+)$ population process *in the afterglow* has been demonstrated in figure 5, where the decay rate of $N_2^+(B^2\Sigma_u^+, v = 0)$ state slower than expected one is seen. However, additional population channel *during the discharge* can be still hidden due to additional depopulation channel (quenching by electrons).

To determine time instant, when the additional population becomes noticeable, the dynamics of rotational temperature of $N_2^+(B^2\Sigma_u^+, v = 0)$ state is used. According to [51, 52] at least 4-5 collisions are required for relaxation of rotational distribution in nitrogen at $T = 300 - 900$ K. Due to high quenching rate constant of $N_2^+(B^2\Sigma_u^+, v = 0)$ state [16, 18] such relaxation does not occur at present conditions and the rotational distribution of $N_2^+(B^2\Sigma_u^+, v = 0)$ state formed during its population is conserved. Since rotational constants of $N_2(X^1\Sigma_g^+)$ and nitrogen ion are close [53], rotational temperature of $N_2^+(B^2\Sigma_u^+, v = 0)$ state is close to the gas temperature, if the state is populated by electron impact from nitrogen ground state (5). Additional processes of $N_2^+(B^2\Sigma_u^+, v = 0)$ population can perturb $N_2^+(B^2\Sigma_u^+, v = 0)$ rotational distribution sufficiently. In this case, rotational temperature of $N_2^+(B^2\Sigma_u^+, v = 0)$ state is significantly different from the gas temperature. This fact can be used to identify the time instant when role of the additional population channels becomes determinant. The spectra presented in figure 13 and figure 14 show noticeable deformation of FNS(0-0) shape after 20 ns: tail of the FNS(0-0) band starts to flatten. At 30 ns the bump seen before at 390.5 nm disappear completely indicating strong rotational redistribution.

In order to check the appearance of an additional $N_2^+(B^2\Sigma_u^+, v = 0)$ population processes rotational temperatures of $N_2^+(B^2\Sigma_u^+, v = 0)$ and $N_2(C^3\Pi_u, v' = 1)$ are compared at the beginning of the discharge pulse and at 30 ns. The results are presented in figure 11, where the spectra of FNS(0-0) and SPS(1-4) are fitted by SpecAir [38] software. At the beginning of the discharge both states provide the gas temperature of 380 K, which is in perfect agreement with the previous studies [29]. Please note that in order to obtain the gas temperature the rotational temperature of the $N_2(C^3\Pi_u)$ state is multiplied by ratio between rotational constants of the $N_2(X^1\Sigma_g^+)$ and $N_2(C^3\Pi_u)$ states ($B_e^X/B_e^C = 1.998/1.825 = 1.095$ [53]). At 30 ns the rotational temperature of $N_2^+(B^2\Sigma_u^+, v = 0)$ is about 900 K, while the gas temperature determined by $N_2(C^3\Pi_u, v' = 1)$ is 420 K only. To confirm that population of the $N_2(C^3\Pi_u)$ state can be used to determine the gas temperature, i.e. it is populated from the ground state of molecular nitrogen, a relative vibrational population of the $N_2(C^3\Pi_u)$ state is considered. The spectra similar to the ones shown in figure 2 are recorded at different time instants with the camera gate of 3 ns and intensities, $I_{v-v'}$, of $(v - v')$ transitions of the SPS are obtained by integration over the wavelength. The sequence with $\Delta v = 2$ is used. Then the relative vibrational population of the $N_2(C^3\Pi_u)$ state is calculated by

$$\frac{[N_2(C^3\Pi_u, v)]}{[N_2(C^3\Pi_u, 0)]} = \frac{I_{v-v'}}{I_{0-2}} \cdot \frac{A_{vv'}}{A_{02}}, \tag{6}$$

where $A_{vv'}$ is an Einstein coefficient of $(v - v')$ transition of SPS. The dynamics of

the relative vibrational population of the $N_2(C^3\Pi_u)$ state is presented in figure 12. At the beginning of the discharge pulse vibrational population of the $N_2(C^3\Pi_u)$ state is in a good agreement with the theoretically calculated population corresponding to the excitation from $N_2(X^1\Sigma_u, v'=0)$ by electron impact proportional to F_{v0}/F_{00}, where $F_{vv'}$ is a corresponding Frank-Condon factor of $N_2(C^3\Pi_u, v) \rightarrow N_2(X^1\Sigma_u, v')$ transition [54]. A good agreement is clearly seen between the experimentally measured vibrational distribution at the beginning of the discharge pulse (6 ns) and the distribution corresponding to the excitation from $N_2(X^1\Sigma_u, v'=0)$. Then vibrational distribution deforms: intensive population of levels $v = 3, 4$ is clearly seen in figure 12. Such vibrational distribution (26 ns) is in a good agreement with an *estimate* made in assumption that $N_2(C^3\Pi_u)$ is populated from vibrationally excited $N_2(X^1\Sigma_u)$ with vibrational temperature of 3000 K, see figure 12. At the end of the discharge pulse (after 26 ns), vibrational relaxation of $N_2(C^3\Pi_u, v)$ is observed. Thus, it can be concluded that the $N_2(C^3\Pi_u)$ state is populated from the ground state of nitrogen and can be used to determine the gas temperature.

(a) **(b)**

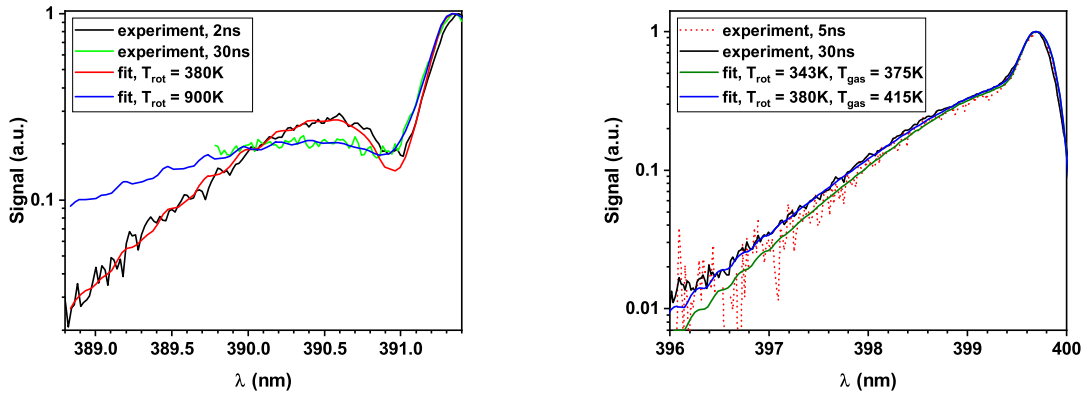

Figure 11. Experimentally measured spectra of (a) FNS(0-0) and (b) SPS(1-4) transitions together with SpecAir [38] fits used to determine rotational temperature of the excited states. At the beginning of the discharge pulse both species show gas temperature of about 380 K, while at 30 ns rotational temperature of $N_2^+(B^2\Sigma_u^+, v=0)$ states is more than 2 times higher than the gas temperature, see text. Entrance slit of 100 μm, 1200 l/mm grating, averaging of 200 accumulations.

Strong deviation of ion rotational temperature from the gas temperature, see figure 11, confirms presence of additional process of $N_2^+(B^2\Sigma_u^+, v=0)$ population. As it was mentioned, shape of the FNS(0-0) spectra shown in figures 13-14 suggests that the additional population becomes important at about 30 ns.

At $E/N \leq 160$ Td and ionization degree typical for the present work, the excitation of the ground state of ion by electron impact

$$N_2^+(X^2\Sigma_g^+, v'=0) + e \rightarrow N_2^+(B^2\Sigma_u^+, v''=0) + e, \qquad (7)$$

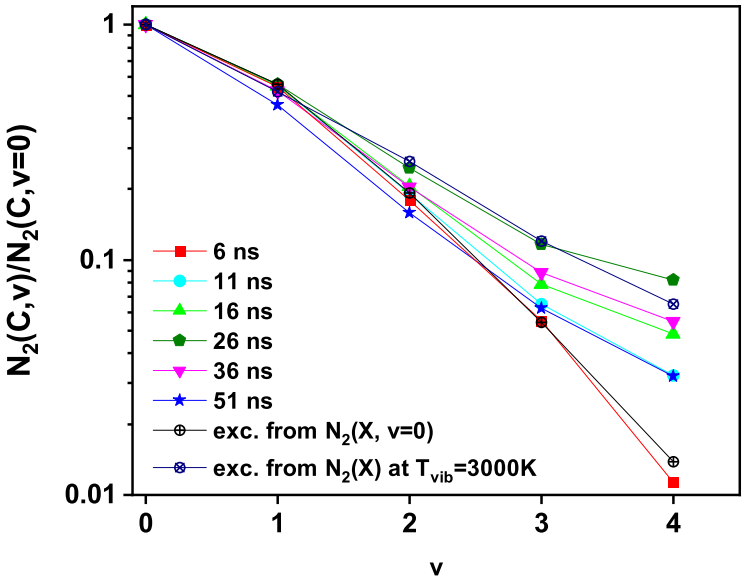

Figure 12. Dynamics of the relative vibrational population of the $N_2(C^3\Pi_u)$ state measured experimentally together with the vibrational population corresponding to the excitation from the ground state of nitrogen with vibrational temperature of 300 K and 3000 K, see text.

becomes comparable to the process (5) that is fundamental for the OES *E*-field technique.

The cross-section of process (7) is taken from [50] and the Franck–Condon factor equal to 0.663 is taken from [54].

The main processes providing a sufficient for the reaction (7) density of nitrogen ions in the ground state, $N_2^+(X^2\Sigma_g^+)$, are ionization by direct electron impact,

$$N_2(X^1\Sigma_g^+) + e \to N_2^+(X^2\Sigma_g^+) + e + e \tag{8}$$

during the discharge, and Penning ionization in collisions of electronically excited $N_2(a'^1\Sigma_u^-)$ molecules *in early afterglow* [27]:

$$N_2(a'^1\Sigma_u^-) + N_2(a'^1\Sigma_u^-) \to N_2^+(X^2\Sigma_g^+) + N_2 + e. \tag{9}$$

Meanwhile, the decay of the density of the molecular ion in the ground state is slow, the $[N_2^+(X^2\Sigma_g^+)]$ decreases by a factor of 2 during approximately 25 ns (see the dashed black curve in figure 10). The main reactions responsible for the decay are the electron-ion dissociative recombination

$$N_2^+ + e \to N(^4S) + N(^2D, ^2P) \tag{10}$$

and 3-body conversion of N_2^+ to complex N_4^+ ions [55]

$$N_2^+ + N_2 + N_2 \rightarrow N_4^+ + N_2 \tag{11}$$

with $k_{11} = 6.2 \cdot 10^{-29} \cdot (300/T)^{1.7}$ cm^{6}s^{-1} [56]. Although the role of the reaction of conversion (11) is crucial at atmospheric pressure, lowering the pressure to 27 mbar and increase of the gas temperature up to 600 K [29] assures a small degree of conversion: the ratio $[N_4^+]/[N_2^+] \lesssim 0.1$ is constant at the time interval 10-60 ns. Further decrease of the ratio $[N_4^+]/[N_2^+]$ caused by significant acceleration of the reaction reverse to (11) [56, 57] at gas temperature increase [29] also should be noted.

As a result, the density of N_2^+ is significant during the whole considered interval of the discharge and early afterglow, $[N_2^+]/[N_2] \approx 3 \cdot 10^{-4} - 10^{-3}$, and thus, the additional population (7) of $N_2^+(B^2\Sigma_u^+, v = 0)$ state from the ground state of the ion is important.

Including the reaction (7) provides a good agreement of the density of the upper level of the FNS with the experimental data at the time interval $t \lesssim 40$ ns, see dashed curve 1 in figure 10.

Later, at $t \gtrsim 40$ ns the calculated FNS intensity decreases further, while the measured intensity almost does not change, see figures 5 and 14. This indicates that there is at least one more channel of the $N_2^+(B^2\Sigma_u^+, v = 0)$ population, active mainly in the afterglow.

As far as the decay of $N_2^+(X^2\Sigma_g^+)$ density is slow, tens of nanoseconds, it is possible that $N_2^+(B^2\Sigma_u^+, v = 0)$ state is excited from the ground state of N_2^+ ion in collisions with heavy particles. In this work, it is assumed that this process is a reaction with excited $N_2(A^3\Sigma_u^+)$ molecules efficiently produced [29] in the discharge:

$$N_2^+(X^2\Sigma_g^+) + N_2(A^3\Sigma_u^+) \rightarrow N_2^+(B^2\Sigma_u^+, v') + N_2(X^1\Sigma_g^+, v''). \tag{12}$$

A solid curve 2 in figure 10 corresponds to the numerical calculations of the FNS dynamics taking into account both the excitation by electron impact from the ground state of molecular ion (7) and the suggested reaction (12) with the rate constant $k_{12} = 4 \cdot 10^{-10}$ cm^{3}s^{-1}. It is clearly seen that including process (12) allows to reproduce numerically the behavior of 1^--system of nitrogen observed experimentally.

It is noted in [57] that the reaction (12) can proceed in two stages:

$$N_2^+(X^2\Sigma_g^+) + N_2(A^3\Sigma_u^+) \rightarrow N_3^+ + N(^4S), \tag{13}$$

$$N_3^+ + N(^4S) \rightarrow N_2^+(B^2\Sigma_u^+, v') + N_2(X^1\Sigma_g^+, v'') \tag{14}$$

with the rate constant of the first reaction $k_{13} \leq 3 \cdot 10^{-10}$ cm^{3}s^{-1}, which is in a good agreement with value of k_{12} obtained based on comparison of experimental results with the results of numerical kinetic modeling. Thus, the reaction (12) can control the population of the excited state of the molecular ion in the early afterglow of pulsed discharges with high specific deposited energies and high density of the electronically excited states. Together with (5) they influence the population of the $N_2^+(B^2\Sigma_u^+, v = 0)$ leading to additional overestimation of I_{FNS}/I_{SPS} value causing extremely high but non correct in this case values of reduced electric field if calculated by OES-technique (1).

At conditions different from the considered one, other mechanisms of additional $N_2^+(B^2\Sigma_u^+)$ population can be important. For example, in low-pressure DC discharges at high vibrational excitation of $N_2(X^1\Sigma_g^+, v')$ the reaction

$$N_2^+(X^2\Sigma_g^+) + N_2(X^1\Sigma_g^+, v \geq 11) \rightarrow N_2^+(B^2\Sigma_u^+) + N_2(X^1\Sigma_g^+) \tag{15}$$

plays significant role [57–59], while in the afterglow of nitrogen atmospheric pressure inductively coupled plasma torch [25] at high gas temperature (4000-5000 K) and high nitrogen dissociation degree, the reactions with atomic nitrogen and atomic N^+ ions are important. Please also refer to the introduction of the present paper, where a few other examples of additional population of $N_2^+(B^2\Sigma_u^+)$ were already mentioned.

It should be noted that decrease of density of molecular ions in the ground state, $[N_2^+(X^2\Sigma_g^+)]$, can extend the region of validity of the OES technique for the measurements of the electric field. A possible approach based on kinetics, is to add trace amounts of gases providing a fast charge exchange, like molecular oxygen, water or NO. The charge exchange is characterized by high rate constants:

$$N_2^+ + NO \rightarrow N_2 + NO^+, \tag{16}$$

$$N_2^+ + H_2O \rightarrow N_2 + H_2O^+, \tag{17}$$

with $k_{16} = 4 \cdot 10^{-10}$ cm^{3}s^{-1} and $k_{17} = 2.2 \cdot 10^{-9}$ cm^{3}s^{-1} respectively [60], and so even small densities of NO and H_2O will decrease the N_2^+ density significantly.

Summarizing the discussion presented above, will note that OES technique in applications for the E-field measurements requires a preliminary analysis of the channels of population and decay of electronic states taken into account. If the kinetic is complex, an advanced numerical model should be developed. The gas pressure and temperature are not the only conditions to consider when building the model. There are "hidden" discharge parameters, as for example, specific energy deposition leading to more complex plasma kinetics. At high specific deposited energy, processes between charged/excited/atomic particles become especially efficient. The threshold of the transformation is individual and hardly can be predicted in advance for a given experimental case. However, the temporal behavior of the excited state emission can be used as a simple check, see figure 5. In addition to the decays of $N_2^+(B^2\Sigma_u^+)$ and $N_2(C^3\Pi_u)$ states, other species can be examined. For example, in [29] the temporal evolution of the intensity of the first positive system (FPS) of nitrogen, $N_2(B^3\Pi_g, v') \rightarrow N_2(A^3\Sigma_u^+, v'')$, was used as an indicator of pair processes between excited particles. Analysis of the rotational structure of the optical transitions can be used as a tool to detect presence of additional population processes too.

Depending on the discharge conditions, processes of a noticeable additional population/depopulation of $N_2^+(B^2\Sigma_u^+)$ and $N_2(C^3\Pi_u)$ states should be taken into account to provide the correct field value by E/N measurements based on FNS and SPS intensities ratio. More generally, all spectroscopic techniques can be influenced by such additional processes not accounted in the kinetics scheme, for example, see [61],

where the influence of complex plasma kinetics on actinometry of atomic oxygen in a capillary nanosecond discharge is studied.

6. Conclusions

Analysis of optical emission spectroscopy in application to the measurements of the electric field has been performed for the nanosecond capillary discharge in molecular nitrogen at moderate gas pressure, 27 mbar. It is shown that special attention is needed when using the OES technique for the measurements of the electric field.

It is recommended to perform a separate analysis of temporal behavior of the emission intensity of two selected molecular bands prior to analysis the ratio of the intensities. A special attention should be paid to the decay rates: if they do not correspond to the decay related to the radiative lifetime and quenching by the main components of the gas mixture, processes responsible for it this should be taken into account.

It is also suggested to use rotational structure of selected molecular bands in order to identify the moment of appearing of population processes additional to the population by electron impact from the ground state. The significant discrepancy of $N_2^+(B^2\Sigma_u^+)$ rotational temperature from the gas temperature is demonstrated indicating additional $N_2^+(B^2\Sigma_u^+)$ population channel during the discharge pulse.

At conditions of the present work, only kinetic calculations taking into account additional quenching of $N_2(C^3\Pi_u)$ state by electrons, additional population $N_2^+(B^2\Sigma_u^+)$ by electron impact from the ground state of the molecular ion and by a reaction of excited $N_2(A^3\Sigma_u^+)$ with the ground state of N_2^+ describes adequately behavior of emission of both considered systems.

Additional processes of population and depopulation of the excited states not only prevent the correct measurements of the electric field by the OES technique, but influence other spectroscopic techniques, as actinometry or LIF/TALIF. The processes of collisions of electronically excited or ionized species with electrons and other excited species should always be taken into account for the plasmas with high degrees of electronic excitation, or in other words, for the plasmas with high electric fields and high specific deposited energies.

Acknowledgements

The work was partially supported by LabEx Plas@Par, the French National Research Agency, ANR (ASPEN Project, “Atomic Species Production via Electronically excited states in high eNergy density Plasmas”), DGA-Ecole Polytechnique Convention 2790, LabEx Plas@Par and the French-Russian international laboratory LIA KaPPA ”Kinetics and physics of pulsed plasmas and their afterglow”. During manuscript preparation NL was partially supported by the DFG funded SFB1316 Project ”Transient atmospheric plasmas - from plasmas to liquids to solids”. The work of NP is supported by the

Russian Science Foundation, project no. 19-17-00183. The authors are thankful to Ali Mahjoub and Bruno Dufour for the technical assistance.

Appendix A

The spectra of the FNS(0-0) and SPS(2-5) bands in the time interval $1-30$ and $31-55$ ns are shown in figures 13-14. The amplitude of the FNS(0-0) transition increases during the first two nanoseconds, after it decreases in the interval $2-6$ ns and then increases again. The intensity of emission of the FNS(0-0) transition dominates the one of the SPS(2-5) transition during the first ten nanoseconds, see figures 13(a),(b).
Only at 10-11 ns the emission of the FNS(0-0) and SPS(2-5) bands become comparable. Then, the signals increase synchronously with almost constant ratio of the emission intensities before 21 ns, see figures 13(c),(d). Starting from 21 ns, the decay of the both bands is observed. The emission of the FNS(0-0) band decays faster than the emission of the SPS(2-5) band, see figure 13(f) and figures 14(a),(b). However, at 40 ns the decay of the FNS(0-0) transition slows down dramatically, while the intensity of the SPS(2-5) transition continues to decay, see figure 14(c),(d) and (e).

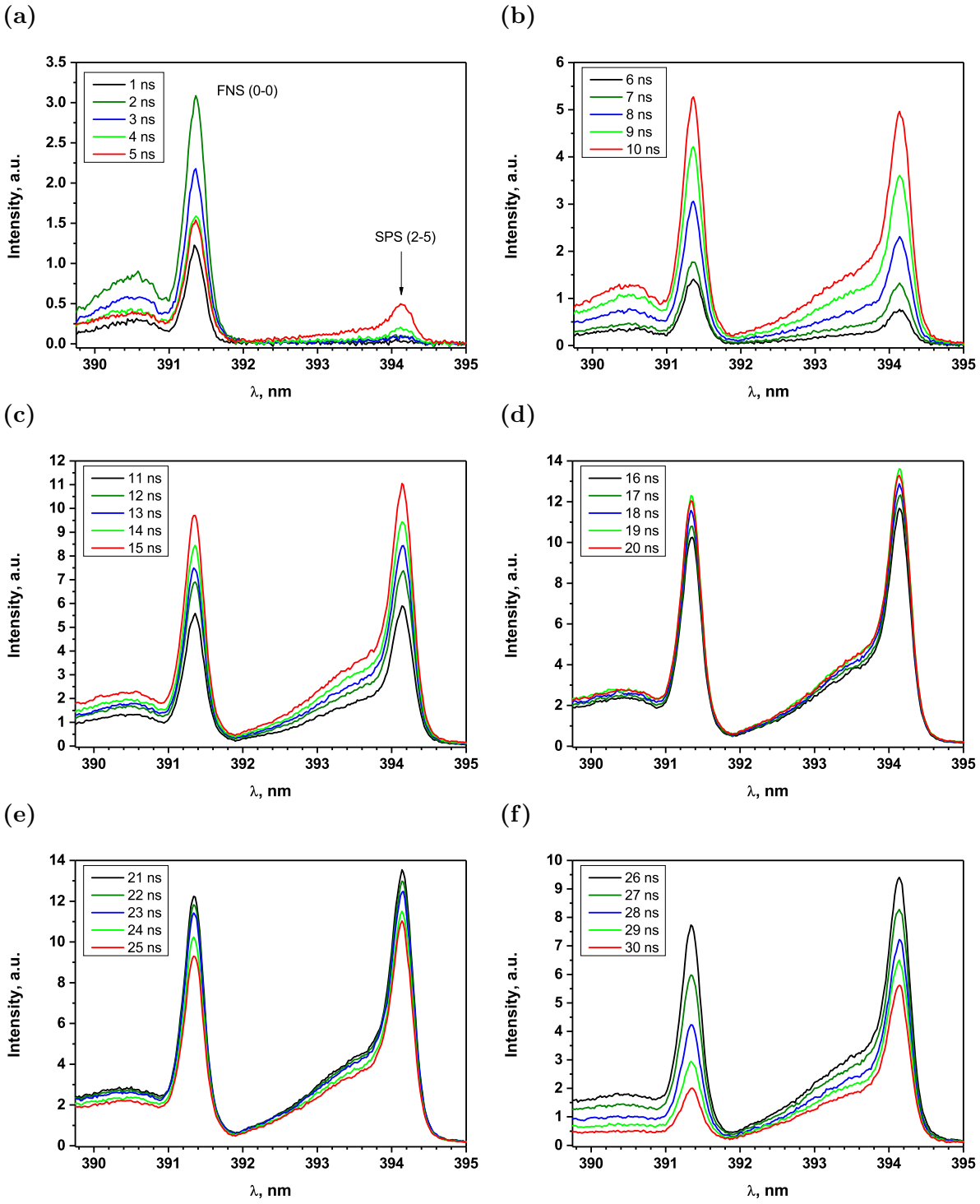

Figure 13. The SPS(2-5) and FNS(0-0) transitions in the time interval 1-30 ns. Pure nitrogen, 27 mbar. Entrance slit of 100 μm, 1200 l/mm grating, averaging of 200 accumulations.

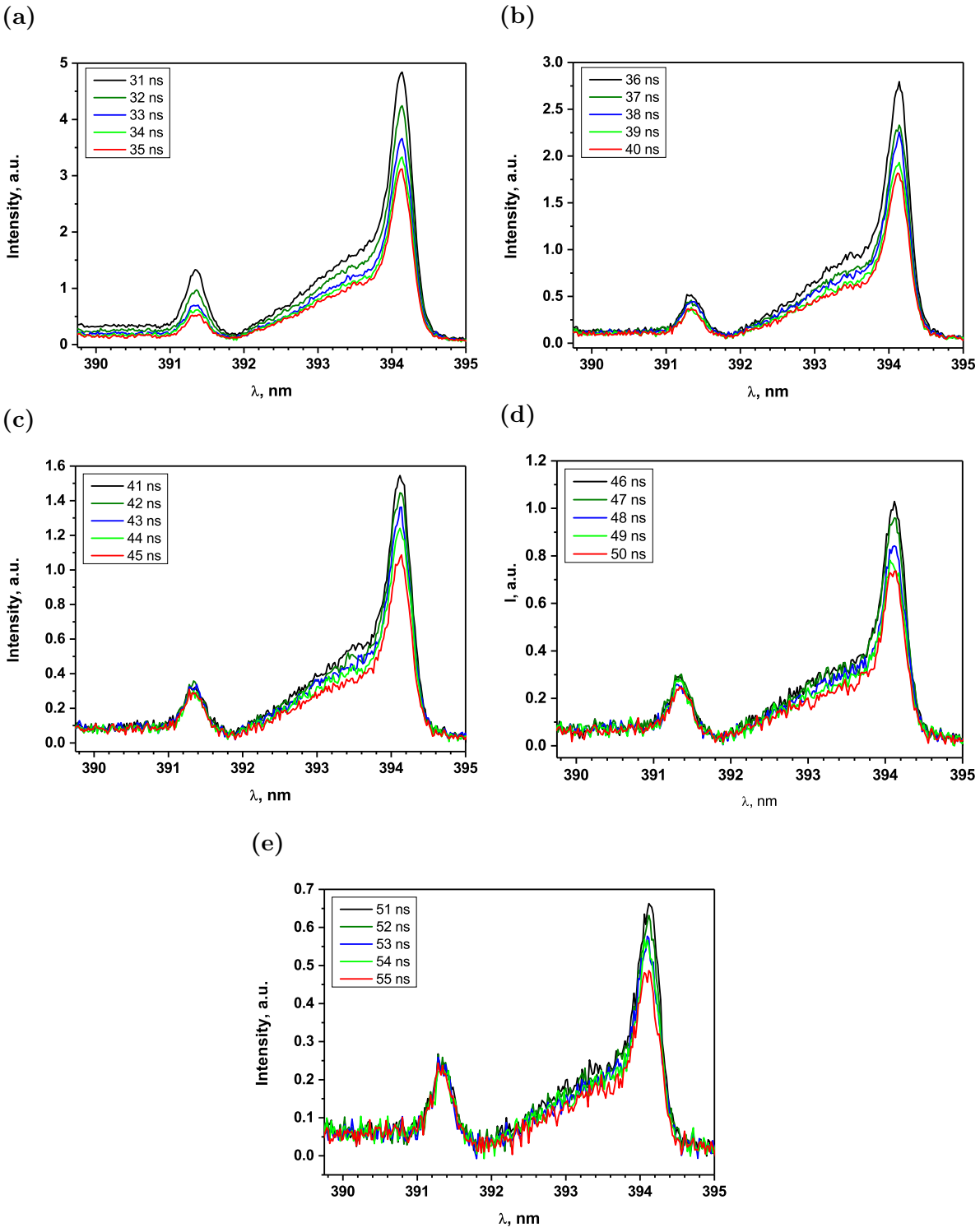

Figure 14. The SPS(2-5) and FNS(0-0) transitions in the time interval 31-55 ns. Pure nitrogen, 27 mbar. Entrance slit of 100 μm, 1200 l/mm grating, averaging of 200 accumulations.

Appendix B

In this section the intensities ratio R_{391}/R_{337} in steady state electric field is calculated and compared with the results of the measurements of [13]. The results are presented in figure 15.

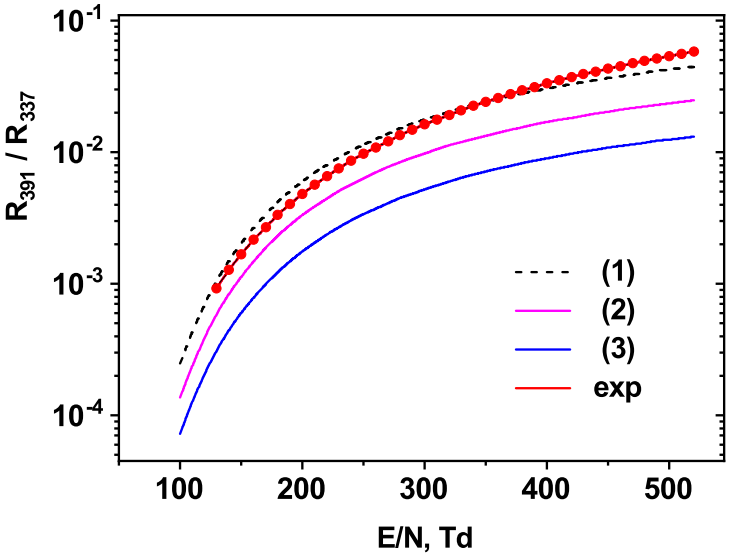

Figure 15. Relative intensity of emission of (0-0) transitions of FNS and SPS, R_{391}/R_{337}, in air. Symbols are the experimental results of [13], curves (1)-(3) are the results of the numerical calculations with different sets of the quenching rate constants of the $N_2^+(B^2\Sigma_u^+)$ state: (1) N_2 - $2.1 \cdot 10^{-10}$cm^{3}s^{-1}, O_2 - $5.1 \cdot 10^{-10}$cm^{3}s^{-1} [18]; (2) N_2 - $4.5 \cdot 10^{-10}$cm^{3}s^{-1}, O_2 - $7.0 \cdot 10^{-10}$cm^{3}s^{-1} [62]; (3) N_2 - $8.84 \cdot 10^{-10}$cm^{3}s^{-1}, O_2 - $10.45 \cdot 10^{-10}$cm^{3}s^{-1} [63].

One can see that the best agreement with the experimental results [13] is achieved if the set from [18] used. This justifies the choose of the collisional quenching rate $k_q^B = 2.1 \cdot 10^{-10}$cm^{3}s^{-1} [18] used for the reduced electric field calculations, see figures 6-7. It also confirms that increased value of the collisional quenching frequency of the $N_2^+(B^2\Sigma_u^+)$ state, $k_q^B = 7 \cdot 10^{-10}$cm^{3}s^{-1} used for the numerical calculations, see figure 10 and the corresponding discussion, is caused by an additional depopulation process appearing at conditions of high specific deposited energy at high reduced electric fields.

References

[1] Gallimberti I, Hepworth J K and Klewe R C 1974 Spectroscopic investigation of impulse corona discharges *Journal of Physics D: Applied Physics* **7** 880–898

[2] Spyrou N and Manassis C 1989 Spectroscopic study of a positive streamer in a point-to-plane discharge in air: evaluation of the electric field distribution *Journal of Physics D: Applied Physics* **22** 120–128

[3] Kozlov K V, Wagner H E, Brandenburg R and Michel P 2001 Spatio-temporally resolved spectroscopic diagnostics of the barrier discharge in air at atmospheric pressure *Journal of Physics D: Applied Physics* **34** 3164–3176

[4] Bílek P, Šimek M and Bonaventura Z 2019 Electric field determination from intensity ratio of N_2^+ and N_2 bands: nonequilibrium transient discharges in pure nitrogen *Plasma Sources Science and Technology* **28** 115011

[5] Pancheshnyi S V, Starikovskaia S M and Starikovskii A Y 1999 Population of nitrogen molecule electron states and structure of the fast ionization wave *Journal of Physics D: Applied Physics* **32** 2219

[6] Anikin N B, Starikovskaia S M and Starikovskii A Y 2002 Polarity effect of applied pulse voltage on the development of uniform nanosecond gas breakdown *Journal of Physics D: Applied Physics* **35** 2785

[7] Goldberg B M, Chng T L, Dogariu A and Miles R B 2018 Electric field measurements in a near atmospheric pressure nanosecond pulse discharge with picosecond electric field induced second harmonic generation *Applied Physics Letters* **112** 064102

[8] Stepanyan S A, Starikovskiy A Y, Popov N A and Starikovskaia S M 2014 A nanosecond surface dielectric barrier discharge in air at high pressures and different polarities of applied pulses: transition to filamentary mode *Plasma Sources Science and Technology* **23** 045003

[9] Naidis G V 2009 Positive and negative streamers in air: Velocity-diameter relation *PRE* **79** 057401

[10] Bonaventura Z, Bourdon A, Celestin S and Pasko V P 2011 Electric field determination in streamer discharges in air at atmospheric pressure *Plasma Sources Science and Technology* **20** 035012

[11] Hoder T, Bonaventura Z, Bourdon A and Šimek M 2015 Sub-nanosecond delays of light emitted by streamer in atmospheric pressure air: Analysis of $N_2(C^3\Pi_u)$ and $N_2^+(B^2\Sigma_u^+)$ emissions and fundamental streamer structure *Journal of Applied Physics* **117** 073302

[12] Hoder T, Loffhagen D, Voráč J, Becker M M and Brandenburg R 2016 Analysis of the electric field development and the relaxation of electron velocity distribution function for nanosecond breakdown in air *Plasma Sources Science and Technology* **25** 025017

[13] Paris P, Aints M, Valk F, Plank T, Haljaste A, Kozlov K V and Wagner H E 2005 Intensity ratio of spectral bands of nitrogen as a measure of electric field strength in plasmas *Journal of Physics D: Applied Physics* **38** 3894

[14] Brisset A, Gazeli K, Magne L, Pasquiers S, Jeanney P, Marode E and Tardiveau P 2019 Modification of the electric field distribution in a diffuse streamer-induced discharge under extreme overvoltage *Plasma Sources Science and Technology* **28** 055016

[15] Paris P A M and F V 2009 *Book of Contributed Papers, 17th Symp. on Application of Plasma Processes and Visegrad Workshop on Research of Plasma Physics (Liptovsky Jan, Slovakia, 17–22 January)* p 227

[16] Valk F, Aints M, Paris P, Plank T, Maksimov J and Tamm A 2010 Measurement of collisional quenching rate of nitrogen states $N_2(C^3\Pi_u, v = 0)$ and $N_2^+(B\,^2\Sigma_g^+, v = 0)$ *Journal of Physics D: Applied Physics* **43** 385202

[17] Hoder T, Šimek M, Bonaventura Z, Prukner V and Gordillo-Vázquez F J 2016 Radially and temporally resolved electric field of positive streamers in air and modelling of the induced plasma chemistry *Plasma Sources Science and Technology* **25** 045021

[18] Pancheshnyi S, Starikovskaia S and Starikovskii A 1998 Measurements of rate constants of the $N_2(C^3\Pi_u, v' = 0)$ and $N_2^+(B^2\Sigma_u^+, v' = 0)$ deactivation by N_2, O_2, H_2, CO and H_2O molecules

in afterglow of the nanosecond discharge *Chemical Physics Letters* **294** 523 – 527

[19] Pancheshnyi S, Starikovskaia S and Starikovskii A 2000 Collisional deactivation of $N_2(C^3\Pi_u,\ v = 0, 1, 2, 3)$ states by N_2, O_2, H_2 and H_2O molecules *Chemical Physics* **262** 349 – 357

[20] Obrusník A, Bílek P, Hoder T, Šimek M and Bonaventura Z 2018 Electric field determination in air plasmas from intensity ratio of nitrogen spectral bands: I. Sensitivity analysis and uncertainty quantification of dominant processes *Plasma Sources Science and Technology* **27** 085013

[21] Bílek P, Obrusník A, Hoder T, Šimek M and Bonaventura Z 2018 Electric field determination in air plasmas from intensity ratio of nitrogen spectral bands: II. Reduction of the uncertainty and state-of-the-art model *Plasma Sources Science and Technology* **27** 085012

[22] Popov N A 2011 Kinetic processes initiated by a nanosecond high-current discharge in hot air *Plasma Physics Reports* **37** 807

[23] Pothiraja R, Ruhrmann C, Engelhardt M, Bibinov N and Awakowicz P 2013 Characterization of atmospheric-pressure ac micro-discharge in He–N_2 mixture using time- and space-resolved optical emission spectroscopy *Journal of Physics D: Applied Physics* **46** 464012

[24] Gröger S, Ramakers M, Hamme M, Medrano J A, Bibinov N, Gallucci F, Bogaerts A and Awakowicz P 2018 Characterization of a nitrogen gliding arc plasmatron using optical emission spectroscopy and high-speed camera *Journal of Physics D: Applied Physics* **52** 065201

[25] Tibère-Inglesse A C, McGuire S D, Mariotto P and Laux C O 2019 Experimental study of recombining nitrogen plasmas: I. Vibronic population distributions and nonequilibrium molecular radiation *Plasma Sources Science and Technology* **28** 075018

[26] T Orriere N Benard E M and Pai D Z 2019 Electric field and electron density measurements of nanosecond repetitively pulsed microplasmas in atmospheric air *Proc. of 24th International Symposium on Plasma Chemistry (ISPC 24), 9 – 14 June 2019, Naples, ItalyProc. of 24th International Symposium on Plasma Chemistry (ISPC 24), 9 – 14 June 2019, Naples, Italy*

[27] Lepikhin N D, Klochko A V, Popov N A and Starikovskaia S M 2016 Long-lived plasma and fast quenching of $N_2(C^3\Pi_u, v)$ by electrons in the afterglow of a nanosecond capillary discharge in nitrogen *Plasma Sources Science and Technology* **25** 045003

[28] Klochko A V, Starikovskaia S M, Xiong Z and Kushner M J 2014 Investigation of capillary nanosecond discharges in air at moderate pressure: comparison of experiments and 2D numerical modelling *Journal of Physics D: Applied Physics* **47** 365202

[29] Lepikhin N D, Popov N A and Starikovskaia S M 2018 Fast gas heating and radial distribution of active species in nanosecond capillary discharge in pure nitrogen and N_2:O_2 mixtures *Plasma Sources Science and Technology* **27** 055005

[30] Chng T L, Lepikhin N D, Orel I S, Popov N A and Starikovskaia S M 2020 TALIF measurements of atomic nitrogen in the afterglow of a nanosecond capillary discharge *Plasma Sources Science and Technology* **29** 035017

[31] Vasilyak L M, Kostyuchenko S V, Kudryavtsev N N and Filyugin I V 1994 Fast ionisation waves under electrical breakdown conditions *Physics-Uspekhi* **37** 247

[32] Anikin N B, Pancheshnyi S V, Starikovskaia S M and Starikovskii A Y 1998 Breakdown development at high overvoltage: electric field, electronic level excitation and electron density *Journal of Physics D: Applied Physics* **31** 826

[33] Anikin N, Starikovskaia S and Starikovskii A 2004 Study of the oxidation of alkanes in their mixtures with oxygen and air under the action of a pulsed volume nanosecond discharge *Plasma Physics Reports* **30** 1028–1042

[34] Takashima K, Adamovich I V, Xiong Z, Kushner M J, Starikovskaia S, Czarnetzki U and Luggenhölscher D 2011 Experimental and modeling analysis of fast ionization wave discharge propagation in a rectangular geometry *Physics of Plasmas* **18** 083505

[35] Takashima K, Adamovich I V, Czarnetzki U and Luggenhölscher D 2012 Development of Fast Ionization Wave Discharges at High Pulse Repetition Rates *Plasma Chemistry and Plasma Processing* **32** 471–493

[36] Klochko A V, Lemainque J, Booth J P and Starikovskaia S M 2015 TALIF measurements of oxygen

atom density in the afterglow of a capillary nanosecond discharge *Plasma Sources Science and Technology* **24** 025010
[37] Ochkin V N 2009 *Spectroscopy of low temperature plasma* (John Wiley & Sons)
[38] Laux C O, Spence T G, Kruger C H and Zare R N 2003 Optical diagnostics of atmospheric pressure air plasmas *Plasma Sources Science and Technology* **12** 125
[39] Itikawa Y 2005 Cross Sections for Electron Collisions with Nitrogen Molecules *Journal of Physical and Chemical Reference Data* **35** 31–53
[40] Chen X, Zhu Y, Wu Y, Hao J, Ma X and Lu P 2021 Modeling of fast ionization waves in pure nitrogen at moderate pressure *Plasma Sources Science and Technology* **30** 065002
[41] Hagelaar G J M and Pitchford L C 2005 Solving the Boltzmann equation to obtain electron transport coefficients and rate coefficients for fluid models *Plasma Sources Science and Technology* **14** 722
[42] Phelps A V and Pitchford L C 1985 Anisotropic scattering of electrons by N_2 and its effect on electron transport *Phys. Rev. A* **31**(5) 2932–2949
[43] Popov N A 2011 Fast gas heating in a nitrogen-oxygen discharge plasma: I. Kinetic mechanism *Journal of Physics D: Applied Physics* **44** 285201
[44] Mintoussov E I, Pendleton S J, Gerbault F G, Popov N A and Starikovskaia S M 2011 Fast gas heating in nitrogen-oxygen discharge plasma: II. Energy exchange in the afterglow of a volume nanosecond discharge at moderate pressures *Journal of Physics D: Applied Physics* **44** 285202
[45] Popov N 2009 Associative ionization reactions involving excited atoms in nitrogen plasma *Plasma Physics Reports* **35** 436–449
[46] Volynets A V, Lopaev D V, Rakhimova T V, Chukalovsky A A, Mankelevich Y A, Popov N A, Zotovich A I and Rakhimov A T 2018 N2 dissociation and kinetics of N(4S) atoms in nitrogen DC glow discharge *Journal of Physics D: Applied Physics* **51** 364002
[47] Lin X, Tyl C, Naudé N, Gherardi N, Popov N A and Dap S 2020 The role of associative ionization reactions in the memory effect of atmospheric pressure Townsend discharges in N2 with a small O2 addition *Journal of Physics D: Applied Physics* **53** 205201
[48] Popov N 2013 Dissociation of nitrogen in a pulse-periodic dielectric barrier discharge at atmospheric pressure *Plasma Physics Reports* **39** 420–424
[49] Klopovsky K S, Mukhovatova A V, Popov A M, Popov N A, Popovicheva O B and Rakhimova T V 1994 Kinetics of metastable states in high-pressure nitrogen plasma pumped by high-current electron beam *Journal of Physics D: Applied Physics* **27** 1399
[50] Bacri J and Medani A 1982 Electron diatomic molecule weighted total cross section calculation: III. Main inelastic processes for N_2 and N_2^+ *Physica B+C* **112** 101 – 118
[51] Park C 2004 Rotational Relaxation of N_2 Behind a Strong Shock Wave *Journal of Thermophysics and Heat Transfer* **18** 527–533
[52] Valentini P, Norman P, Zhang C and Schwartzentruber T E 2014 Rovibrational coupling in molecular nitrogen at high temperature: An atomic-level study *Physics of Fluids* **26** 056103
[53] Radzig A A and Smirnov B M 1985 Reference Data on Atoms, Molecules and Ions *Springer, Berlin*
[54] Gilmore F R, Laher R R and Espy P J 1992 Franck-Condon Factors, r-Centroids, Electronic Transition Moments, and Einstein Coefficients for Many Nitrogen and Oxygen Band Systems *Journal of Physical and Chemical Reference Data* **21** 1005–1107
[55] Sieck L W, Heron J T and Green D S 2000 Chemical Kinetics Database and Predictive Schemes for Humid Air Plasma Chemistry. Part I: Positive Ion-Molecule Reactions *Plasma Chemistry and Plasma Processing* **20** 235–258
[56] Kossyi I A, Kostinsky A Y, Matveyev A A and Silakov V P 1992 Kinetic scheme of the non-equilibrium discharge in nitrogen-oxygen mixtures *Plasma Sources Science and Technology* **1** 207
[57] Slovetsky D I 1980 *Mechanisms of chemical reactions in a nonequilibrium plasma* (Moscow: Nauka (in Russian))
[58] Golubovskii Y B and Telezhko V M 1984 Ionization processes in a nitrogen discharge at medium

pressures *High Temperature* **23** 340–328

[59] Levaton J, Amorim J, Souza A, Franco D and Ricard A 2002 Kinetics of atoms, metastable, radiative and ionic species in the nitrogen pink afterglow *Journal of Physics D: Applied Physics* **35** 689

[60] McEwan M J and Phillips L F 1975 *Chemistry of the Atmosphere* (London: Edward Arnold)

[61] Zhu Y, Lepikhin N D, Orel I S, Salmon A, Klochko A V and Starikovskaia S M 2018 Optical actinometry of O-atoms in pulsed nanosecond capillary discharge: peculiarities of kinetics at high specific deposited energy *Plasma Sources Science and Technology* **27** 075020

[62] Hirsh M N, Poss E and Eisner P N 1970 Absolute Fluorescence Yields of 3914-Å Photons from N_2 and Air Excited by Relativistic Electrons *Phys. Rev. A* **1**(6) 1615–1626

[63] Dilecce G, Ambrico P F and Benedictis S D 2010 On the collision quenching of $N_2^+(B^2\Sigma_u^+, v = 0)$ by N_2 and $O_2$and its influence on the measurement of E/N by intensity ratio of nitrogen spectral bands *Journal of Physics D: Applied Physics* **43** 195201